





The Large-scale Coronal Structure of the 2017 August 21 Great American Eclipse: An Assessment of Solar Surface Flux Transport Model Enabled Predictions and Observations

Dibyendu Nandy^{1,2} , Prantika Bhowmik¹, Anthony R. Yeates³ , Suman Panda^{1,2}, Rajashik Tarafder¹, and Soumyaranjan Dash¹

¹Center of Excellence in Space Sciences India, Indian Institute of Science Education and Research Kolkata, Mohanpur 741246, West Bengal, India; dnandi@iiserkol.ac.in

²Department of Physical Sciences, Indian Institute of Science Education and Research Kolkata, Mohanpur 741246, West Bengal, India

³Department of Mathematical Sciences, Durham University, Durham DH1 3LE, UK

Received 2017 September 22; accepted 2017 December 7; published 2018 January 24

Abstract

On 2017 August 21, a total solar eclipse swept across the contiguous United States, providing excellent opportunities for diagnostics of the Sun's corona. The Sun's coronal structure is notoriously difficult to observe except during solar eclipses; thus, theoretical models must be relied upon for inferring the underlying magnetic structure of the Sun's outer atmosphere. These models are necessary for understanding the role of magnetic fields in the heating of the corona to a million degrees and the generation of severe space weather. Here we present a methodology for predicting the structure of the coronal field based on model forward runs of a solar surface flux transport model, whose predicted surface field is utilized to extrapolate future coronal magnetic field structures. This prescription was applied to the 2017 August 21 solar eclipse. A post-eclipse analysis shows good agreement between model simulated and observed coronal structures and their locations on the limb. We demonstrate that slow changes in the Sun's surface magnetic field distribution driven by long-term flux emergence and its evolution governs large-scale coronal structures with a (plausibly cycle-phase dependent) dynamical memory timescale on the order of a few solar rotations, opening up the possibility for large-scale, global corona predictions at least a month in advance.

Key words: magnetohydrodynamics (MHD) – Sun: activity – Sun: corona – Sun: filaments, prominences – Sun: magnetic fields

1. Introduction

Solar eclipses have been observed since the ancient times and have been objects of awe and wonder for human beings. While that natural reaction to a rare occurrence of nature has not changed over time, we have come to realize the immense potential for scientific investigations that eclipses provide (Habbal et al. 2010). The solar eclipse that occurred on 2017 August 21 was visible across the contiguous United States. This event, dubbed the great American solar eclipse, generated immense interest among the general public and scientists alike. In particular, this event provided excellent opportunities for detailed observations of the Sun's coronal structure. The magnetic field configuration of the Sun's atmosphere plays a role in coronal heating and the origin of solar storms that result in severe space weather. Space weather impacts human technologies in space and on Earth, including satellite operations, telecommunications, GPS navigational networks, and electric power grids (Schrijver et al. 2015). Therefore, observing and understanding coronal magnetic field structures are of crucial importance. However, this remains an outstanding challenge even today due to the very low density and consequently low photon flux from the corona (in comparison to the solar disk). In this light, total solar eclipses—rare events wherein the Sun's bright disk is completely masked by the Moon—provide the best opportunity for ground-based coronal diagnostics.

The Sun's magnetic fields are generated in its interior through a magnetohydrodynamic (MHD) dynamo mechanism (Parker 1955; Charbonneau 2010) from where they buoyantly emerge to form sunspots. In the Sun's convection zone, helical

turbulence twists the magnetic field lines at small-scales, and the Coriolis force tilts the axis of underlying magnetic flux tubes at large scales, such that bipolar sunspots pairs or solar active regions (ARs) emerge with a tilt. Flux transport processes, such as differential rotation, turbulent diffusion, and meridional circulation, redistribute the magnetic flux, driving the surface evolution of the Sun's magnetic fields (Wang et al. 1989; Nandy et al. 2011). Surface flux emergence, its consequent redistribution by flux transport processes drive the evolution of the Sun's coronal magnetic field, which tends to evolve and relax toward a minimum energy state in the low plasma- β corona. The latter nonetheless hosts nonpotential structures that are far from equilibrium. A variety of theoretical modeling techniques, such as Potential Field Source Surface (PFSS) extrapolations, Nonlinear Force-Free Field (NLFFF) extrapolations, magneto-frictional, and full MHD approaches, exist to model the coronal structure. A detailed description of these modeling techniques can be found in Mackay & Yeates (2012). In the absence of routine, quantitative coronal field observations (see e.g., Casini et al. 2017 and references therein), these models are currently relied upon to understand the underlying magnetic field structures that drive coronal dynamics. Efforts are underway to utilize model simulations to generate synthetic polarization profiles for interpreting coronal observations in an effort to marry theory and observation (Gibson et al. 2016).

On the one hand, the prediction of the coronal field structure during total eclipses utilizing theoretical models is a Rosetta stone for interpretation of the white light corona visible during totality. On the other hand, the observationally inferred coronal magnetic field provides constraints on theoretical modeling

efforts. Based on MHD simulations of the solar corona, a prediction of the coronal structure of the 2017 August 21 eclipse was made utilizing relevant photospheric and coronal inputs, as described in Predictive Science Inc.⁴ (see also, Mikić et al. 2007; Downs et al. 2016). These simulations provide details of not only the magnetic structure, but also the temperature and emission profiles of the corona. However, these simulations are numerically extremely resource heavy and are not able to capture the impact of built in memory of the solar corona that accrues from the slow large-scale surface field evolution on timescales of months to years (Lean et al. 2002; Schrijver & De Rosa 2003; Cook et al. 2009). In particular, Schrijver & De Rosa (2003) and Cook et al. (2009) have demonstrated the potential of combining surface flux transport (SFT) models and PFSS in exploring coronal structures.

Here, we present an alternative modeling approach to large-scale coronal structure predictions and confront this with observations of the 2017 August 21 eclipse. We first utilize a data-driven SFT model of the Sun (with century-scale solar AR data assimilation) until 2017 August 16 and forward run this to 2017 August 21 (assuming no further emergence of ARs within this period). Subsequently, we use the SFT-predicted surface field as a bottom boundary condition in a PFSS model to extrapolate the expected coronal fields of the 2017 August 21 solar eclipse. We repeat this procedure for different (prediction) time windows of (AR emergence-free) forward runs up to 2017 August 21 to test for the underlying predictive memory.

2. Data and Methods

2.1. SFT Methodology

The magnetic field evolution on the solar surface is governed by two physical processes: advection due to the large-scale flows and diffusion caused by the turbulent motion of supergranular convective cells. The diffusion results in the flux cancellation among the magnetic field of opposite polarities, whereas advection causes transportation of magnetic flux toward the polar regions of the Sun. This entire process is better known as the Babcock–Leighton (BL) mechanism (Babcock 1961; Leighton 1969). The SFT models (Wang et al. 1989, 2000; van Ballegoijen et al. 1998; Schrijver 2001; Mackay et al. 2002a, 2002b; Cameron et al. 2010; Upton & Hathaway 2014; Hickmann et al. 2015) are quite successful in capturing the physics of the BL mechanism. For the constant diffusivity, the magnetic field evolution on the solar surface is governed by the magnetic induction equation,

$$\frac{\partial \mathbf{B}}{\partial t} = \nabla \times (\mathbf{v} \times \mathbf{B}) + \eta \nabla^2 \mathbf{B} \quad (1)$$

where \mathbf{v} represents the large-scale velocities, i.e., the meridional circulation and the differential rotation present on the solar surface, and the parameter η symbolizes the magnetic diffusivity. Surface magnetic fields are predominantly radial (Wang & Sheeley 1992; Solanki 1993). We therefore consider the radial component of the induction equation in spherical

polar coordinates given by

$$\begin{aligned} \frac{\partial B_r}{\partial t} = & -\omega(\theta) \frac{\partial B_r}{\partial \phi} - \frac{1}{R_\odot \sin \theta} \frac{\partial}{\partial \theta} (v(\theta) B_r \sin \theta) \\ & + \frac{\eta_h}{R_\odot^2} \left[\frac{1}{\sin \theta} \frac{\partial}{\partial \theta} \left(\sin \theta \frac{\partial B_r}{\partial \theta} \right) + \frac{1}{\sin^2 \theta} \frac{\partial^2 B_r}{\partial \phi^2} \right] + S(\theta, \phi, t). \end{aligned} \quad (2)$$

Here, $B_r(\theta, \phi, t)$ is the radial component of magnetic field as a function of the co-latitude (θ) and longitude (ϕ), and R_\odot is the solar radius. The axisymmetric differential rotation and meridional circulation are expressed through $\omega(R_\odot, \theta) \approx \omega(\theta)$ and $v(R_\odot, \theta) \approx v(\theta)$, respectively. The parameter η_h is the effective diffusion coefficient, and $S(\theta, \phi, t)$ is the source term describing the emergence of new sunspots. To represent the surface differential rotation as a function of co-latitudes, we use an empirical profile (Snodgrass 1983): $\omega(\theta) = 13.38 - 2.30 \cos^2 \theta - 1.62 \cos^4 \theta$ (in degrees per day). This profile is validated by helioseismic observations (Schou et al. 1998). For the meridional flow, we utilize a profile prescribed by van Ballegoijen et al. (1998) in our model with a maximum speed of 15 ms^{-1} . We have used a constant diffusion coefficient of $250 \text{ km}^2 \text{ s}^{-1}$, which lies within the values inferred from observations (Schrijver & Zwaan 2000). The SFT model is developed using a spherical harmonics technique which uses all harmonics up to $l = 63$ —corresponding to typical supergranular scales on the solar surface.

2.2. Sunspot Data

Modeling the emergence of sunspots requires knowledge of the following parameters: the time of appearance, the position on the solar surface, and the area associated with the spots. In the SFT simulations, it is assumed that all sunspots appearing on the solar photosphere are Bipolar Active Regions (BMRs) of β type and their tilt is based on their latitudinal position (Jiang et al. 2011). The Royal Greenwich Observatory (RGO) and United States Air Force (USAF)/National Oceanic and Atmospheric Administration (NOAA) database provides the required data on ARs from 1913 August until 2016 September. Using this data, we have calibrated our SFT model by comparing model outputs with the observation. The long-term calibration of SFT models is necessary to render the polar fields correctly.

The data required from 2016 October 1 to 2017 August 16 has been obtained from the Helioseismic and Magnetic Imager (HMI) onboard NASA’s *Solar Dynamic Observatory* (SDO). This necessitates cross-instrument calibration (Muñoz-Jaramillo et al. 2015). The area reported by HMI is higher than what is reported by RGO-NOAA/USAF. Since our SFT simulation is calibrated based on 100 years (starting from 1913) of the RGO-NOAA/USAF data set, we scale down the area reported by HMI by a constant factor of 2.2 to match RGO AR areas. We determine this scaling factor using a linear fit between the area reported by both databases for the overlapping period of nine months (2016 January–September). We note that the relative fluxes (of various BMRs and large-scale structures) are preserved in this method. The flux associated with BMRs are estimated based on an empirical relationship (Sheeley 1966; Dikpati et al. 2006): $\Phi(A) = 7.0 \times 10^{19} A$ Maxwells, where A is the area of the whole sunspot in unit of micro-hemispheres. This

⁴ www.predsci.com/corona/aug2017eclipse/home.php

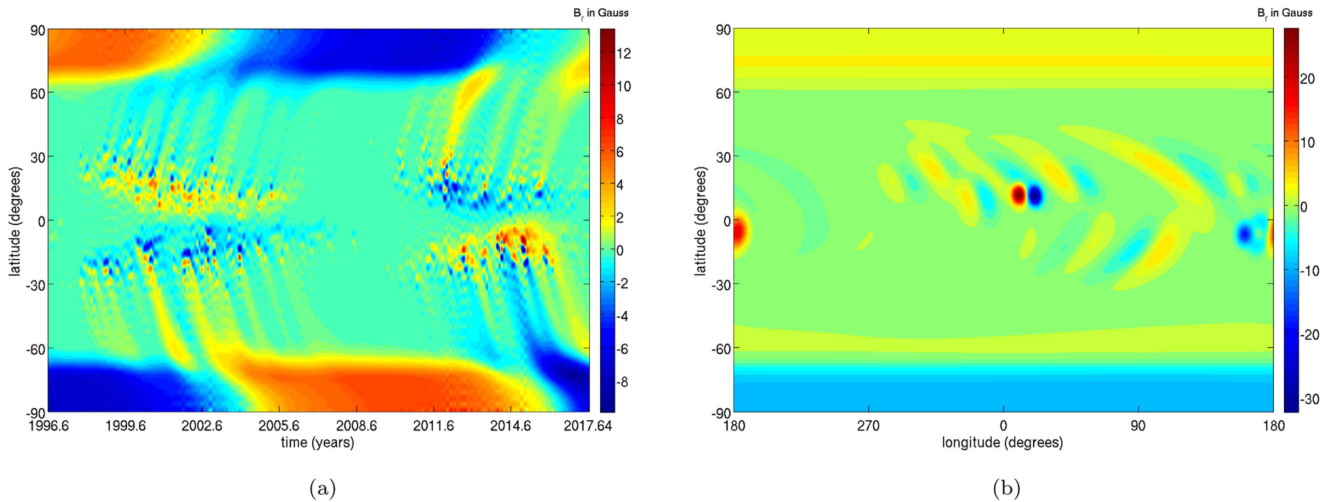


Figure 1. (a) This image depicts the evolution of the solar surface magnetic field during the last decade, generated from our SFT simulation. The last AR was incorporated on 2017 August 16, and the model was forward run to predict the surface map on 2017 August 21. The radial component of longitudinally averaged magnetic field (B_r) is plotted as a function of time and latitude. (b) Shows the simulated photospheric magnetic field distribution (Carrington map) of 2017 August 21.

flux is equally distributed among the two polarities of the BMR. The last AR that was inserted in our SFT model is AR 12671, which emerged at the surface on 2017 August 16.

2.3. PFSS Extrapolation

To generate the coronal magnetic field, we use a PFSS extrapolation model using the photospheric magnetic field as a lower boundary condition (Altschuler & Newkirk 1969; Schatten et al. 1969). This extrapolation assumes a lowest energy (current-free) magnetic field corona. The coronal magnetic field becomes radial at $2.5 R_\odot$ —the upper boundary of our PFSS model—where gas pressure is expected to start dominating over the magnetic pressure (Davis 1965).

3. Results

We use the radial magnetic field data obtained from our SFT simulation to generate the butterfly diagram covering the time from the beginning of solar cycle 23 (1996 May) to 2017 August 21 (Figure 1(a)). In this simulation, the last observed AR was included on 2017 August 16 (AR 12671), and the model was forward run to generate the predicted surface field distribution on 2017 August 21. The large-scale evolution of the solar surface field driven by the AR flux emergence and surface flows is clearly discernible. The last few years of the simulation show the slow poleward migration of “tongues” of the magnetic flux in the approach to the minimum of cycle 24. It is our premise that the structuring and evolution of the large-scale, global coronal field is due to this surface magnetic field evolution with localized (small-scale) perturbations imposed by the emergence of any new ARs whose effects are only apparent after a certain time—equivalent to the dynamical memory in the system. The predicted surface magnetic field (Carrington) map centered around 2017 August 21 (the day of the eclipse) is extracted from this simulation and is depicted in Figure 1(b) (with the solar-disk view depicted in the center-inlay of the first three panels of Figure 2).

This surface magnetic field distribution is then utilized as an input in a PFSS model to extrapolate the global coronal structure expected on 2017 August 21 (Figure 2). The inferred coronal magnetic field structure is our primary and most

important prediction and is shown in Figure 2(a). Only the open field lines reaching up to the source surface are rendered in Figure 2(b). A synthetic coronal white light map, reconstructed using an algorithm that provides more weight (i.e., intensity) to positions with a higher density of projected closed field lines (but without any radial gradient of density), is depicted in Figure 2(c). This SFT–PFSS coupled model predictions include two prominent helmet streamers (regions of closed field lines whose tops reach the source surface) centered below the equator in the southern solar hemisphere, one each in the east and west limb. Their locations (the tip of highest closed loop) are marked as 1 (14° S) and 2 (12° S) in Figure 2(a); their cross-sections appear as voids in Figure 2(b), wherein only open field lines are rendered. A third, more confined and narrow streamer is located in the west limb northern hemisphere (47° N; location 5), whose existence is pinned down in Figure 2(b) (note the narrow localized void at the same location). This third structure is a pseudo-streamer that separates regions of same-polarity coronal holes (Wang et al. 2007; Wang 2015). This is borne out in Figure 3(a), wherein location 5 corresponds to a narrow region of negative polarity in the predicted Carrington map, separating out two positive polarity patches on the solar surface. Regions marked as 3 and 4, in the northern hemisphere west and east limb, respectively, are latitudinally extended as low-lying closed magnetic field structures, which merge with the more prominent streamers (1 and 2) in the synthetic white light corona in Figure 2(c). The coronal region overlying the northern hemisphere east limb is relatively less active compared to the others. Regions marked as 6 and 7 correspond to open field lines associated with polar coronal holes, which appear as unipolar caps in the Carrington maps in Figure 3.

A comparison with the Mauna Loa Solar Observatory coronagraph image acquired on 2017 August 21 (Figure 2(d)) indicates good agreement between the forward-run model prediction and the observed coronal structures. The observations show the existence of 2 broad helmet streamers, the one on the east limb at 18° S and the one on the west limb at 15° S, as well as the narrow elongated pseudo-streamer on the west limb at 46° N.

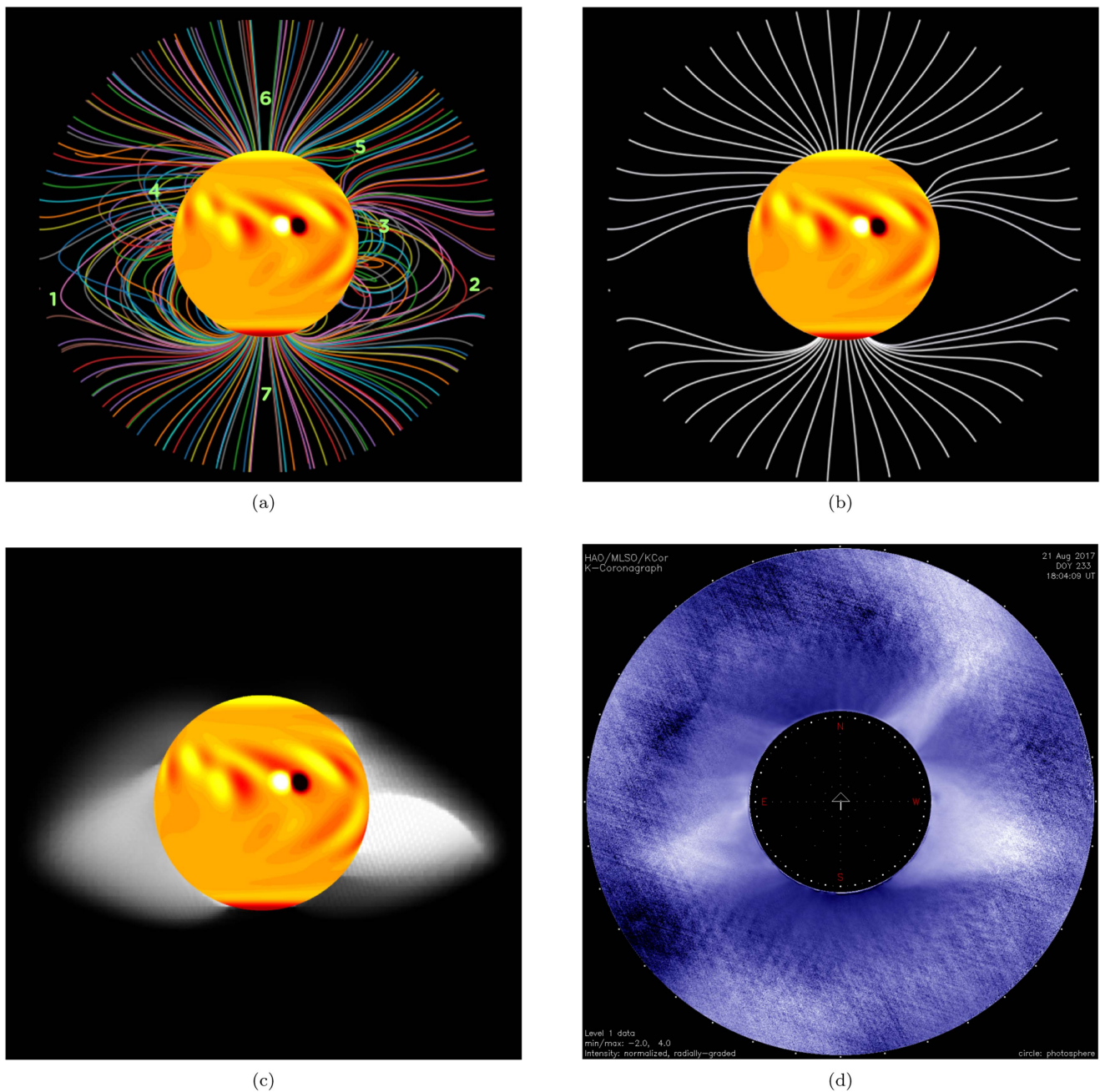


Figure 2. (a) This image depicts a rendering of the open and closed solar coronal magnetic field lines generated using a PFSS model, which utilized the predicted surface magnetic field map from a SFT model forward run to 2017 August 21, i.e., the day of the great American eclipse. (b) Only the open magnetic field lines reaching up to the source surface at $2.5 R_{\odot}$ are depicted. (c) This shows a synthetic map of the white light corona expected during the eclipse rendered using a simplistic algorithm. Thus, this should be interpreted only as a guide-to-the-eye for the latitudinal location of the brightest large-scale coronal structures. (d) This is a K-Cor coronagraph image from Mauna Loa Solar Observatory taken on the day of the solar eclipse. In all of the images, solar north is up.

To test the underlying physical basis of our prediction methodology, namely that the large-scale global coronal structure is a result of long-term surface magnetic field evolution, and to estimate the memory (time window) for predictability, we perform model forward runs to 2017 August 21 without introducing new ARs in the SFT simulation for different time windows (Figure 3). Images in the top panel of Figure 3 show the SFT model-predicted large-scale solar surface polarity separations on 2017 August 21. The only difference in these magnetic maps is in the duration of emergence-free evolution. In case of Figure 3(a), the last AR is inserted in the SFT simulation 24 days before the eclipse, effectively excluding the contributions from 2 ARs, which

appeared in this 24 day period. For Figures 3(b) and (c), the last AR is inserted 54 days (excluding 5 ARs) and 76 days (excluding 8 ARs) prior to 2017 August 21. Images in the middle panel show the corresponding PFSS generated coronal open magnetic field lines. A careful study of the surface polarity distributions and the coronal magnetic field connectivity shows that the 24 days (AR emergence-free) forward-run model-predicted large-scale corona is similar to that predicted 5 days in advance. The forward run for 54 days (i.e., 2 solar rotations) is qualitatively similar with a slight upward shift in the axis of the west limb pseudo-streamer. The 76 days forward run predicted corona shows some differences in the field line connectivity and

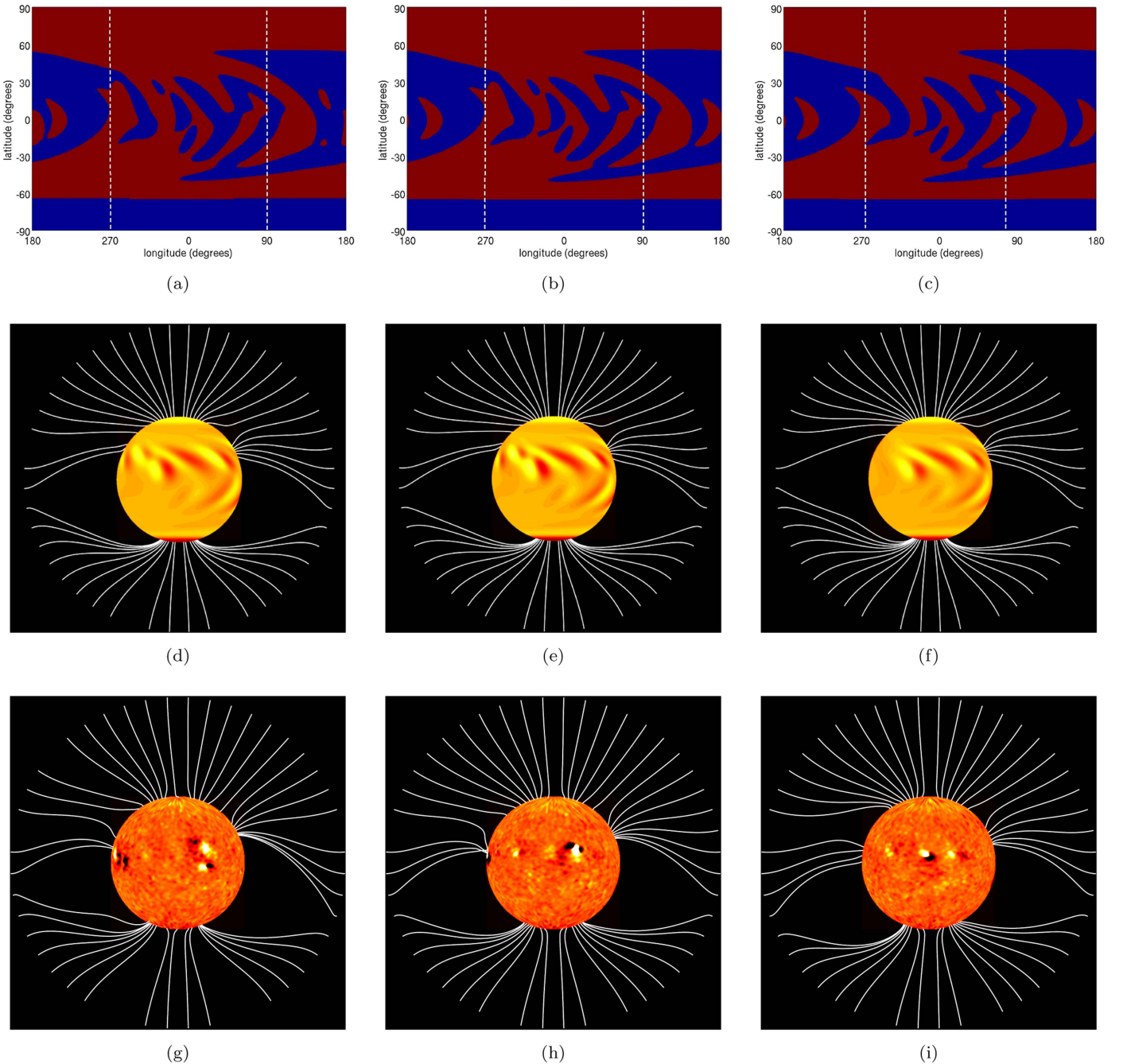


Figure 3. Images in the top panel represent the polarity distribution of the SFT model-predicted surface magnetic field distributions (Carrington maps) for 2017 August 21. The images are color saturated to delineate the locations of neutral lines separating regions of opposite polarity on the Sun’s surface (red: positive polarity, blue: negative polarity). (a) For this prediction run, the last active region input in the SFT simulation is 24 days prior to August 21, i.e., the duration of emergence-free evolution of the surface magnetic field is 24 days. Similarly, for the (b) and (c) prediction runs, the time windows of emergence-free evolution are 54 days and 76 days, respectively. The set of 2 vertical white (dashed) lines at 270° and 90° indicate the east (left) and west (right) limbs of the Sun, respectively. Images in the middle panels (d)–(f) depict coronal open field line structures generated using PFSS extrapolations, corresponding to SFT prediction runs (a)–(c), respectively. Images in the bottom panel of the figure show PFSS extrapolations using daily updated HMI synoptic maps. Panel (g) is generated using observed HMI magnetogram on 2017 July 25, which is one solar rotation prior to the eclipse. For panels (h) and (i), HMI magnetograms corresponding to two and three solar rotations, respectively, before the eclipse are utilized for these PFSS extrapolations.

the latitudinal extent of the (east) limb streamer. We note, however, in spite of these localized differences, that the predicted large-scale shape of the corona during the eclipse is not significantly different. These results indicate a dynamical memory timescale corresponding to two solar rotations in the surface magnetic field evolution induced large-scale solar corona during this (declining) phase of the solar cycle.

We compare the predictive capability of SFT forward run based coronal predictions relative to daily updated HMI synoptic magnetograms corresponding to similar time windows, namely one, two, and three solar rotations before the eclipse. Figure 3 shows that the southern hemisphere west limb streamer generated by the HMI-based extrapolation is somewhat more poleward than was observed (and as predicted by

the SFT-based approach). Moreover, the existence of the northern hemisphere pseudo-streamer could not be clearly identified in the HMI-based extrapolation. We believe these are due to a more accurate determination of the global, large-scale field distribution at high latitudes in the SFT model.

4. Concluding Discussion

In summary, based on data-driven solar SFT simulations forward run to 2017 August 21—the day of the great American solar eclipse—and utilizing the model-predicted solar surface magnetic field maps as inputs to a PFSS model, we have generated simulated coronal structures that were expected to be observed during the eclipse. Post-eclipse comparisons with coronal observations during the eclipse indicate a broad agreement between model-predicted structures and their locations on the solar limb. This agreement supports our conceptual idea of utilizing solar surface magnetic flux transport simulation forward runs to predict the future, large-scale solar corona.

Moreover, through different time windows of (AR emergence-free) model forward runs and PFSS extrapolations, we demonstrate that for the cycle-phase corresponding to the 2017 August 21 eclipse a dynamical memory of about one-to-two solar rotations exists in the system for large-scale global coronal structure predictions. This implies that, utilizing the methodology outlined herein, it is possible to make continuous forecasts of the global coronal structure that are expected one month in the future (and plausibly slightly longer with degrading accuracy). This memory is likely to be cycle-phase dependent; during the solar maximum, it is expected to be less, and closer to the minimum, it is expected to be more. Future investigations will explore this in detail. We also show the clear advantage of this approach over predictions based on synoptic magnetograms acquired a solar rotation (or more) earlier.

We note that our methodology cannot be applied for predictions of small-scale low-lying coronal structures (due to recent AR emergences) or coronal mass ejections. An independent approach based on the Air Force Data Assimilative Photospheric Flux Transport (ADAPT) model (Arge et al. 2010; Henney et al. 2012; Arge et al. 2013; Hickmann et al. 2015) may be more suitable for such purposes for short-term predictions (on a timescale of days). We emphasize that while the eclipse provides an opportunity to compare the model-predicted structures with the observed corona only at the limb, the coupled SFT and PFSS simulations render the global 3D corona and hence predictions for the large-scale corona across all latitudes and longitudes. These simulations—being less-resource-intensive—could therefore be used as an alternative approach for operational long-term, global coronal structure forecasting based on the physical principles outlined above. Future studies will explore the possibility of using the predicted coronal field to generate future solar wind and cosmic ray flux modulations to test the usefulness of this technique beyond predictions of the solar corona.

CESSI is funded by the Ministry of Human Resource Development, Government of India. P.B. acknowledges funding by CEFIPRA/IFCPAR through grant 5004-1. S.D. acknowledges funding from the DST-INSPIRE program of the Government of India. D.N. and A.R.Y. acknowledge the NASA Heliophysics Grand Challenge grant NNX14AO83G for facilitating their interactions. D.N. acknowledges an

associateship from the Inter-University Centre for Astronomy and Astrophysics. We acknowledge utilization of data from the NASA/*SDO* HMI instrument maintained by the HMI team and the Royal Greenwich Observatory/USAF-NOAA active region database compiled by David H. Hathaway. We thank Prosenjit Lahiri and Nabamita Das of CESSI for designing and maintaining the website. We are grateful to an anonymous referee for useful comments that improved a previous version of this work. The CESSI prediction of the coronal field expected during the 2017 August 21 solar eclipse, accompanying images, and data are available at the CESSI solar eclipse prediction website.⁵

ORCID iDs

Dibyendu Nandy  <https://orcid.org/0000-0001-5205-2302>
Anthony R. Yeates  <https://orcid.org/0000-0002-2728-4053>

References

- Altschuler, M. D., & Newkirk, G. 1969, *SoPh*, **9**, 131
Arge, C. N., Henney, C. J., Hernandez, I. G., et al. 2013, in AIP Conf. Ser. 1539, SOLARWIND 13, ed. G. P. Zank et al. (Melville, NY: AIP), 11
Arge, C. N., Henney, C. J., Koller, J., et al. 2010, in AIP Conf. Proc. 1216, SOLARWIND 12, ed. M. Maksimovic et al. (Melville, NY: AIP), 343
Babcock, H. W. 1961, *ApJ*, **133**, 572
Cameron, R. H., Jiang, J., Schmitt, D., & Schüssler, M. 2010, *ApJ*, **719**, 264
Casini, R., White, S. M., & Judge, P. G. 2017, *SSRv*, **210**, 145
Charbonneau, P. 2010, *LRSP*, **7**, 3
Cook, G. R., Mackay, D. H., & Nandy, D. 2009, *ApJ*, **704**, 1021
Davis, L. 1965, in IAU Symp. 22, Stellar and Solar Magnetic Fields, ed. R. Lust (Amsterdam: North-Holland Pub.), 202
Dikpati, M., de Toma, G., & Gilman, P. A. 2006, *GeoRL*, **33**, L05102
Downs, C., Lionello, R., Mikić, Z., Linker, J. A., & Velli, M. 2016, *ApJ*, **832**, 180
Gibson, S., Kucera, T., White, S., et al. 2016, *FrASS*, **3**, 8
Habbal, S. R., Druckmüller, M., Morgan, H., et al. 2010, *ApJ*, **719**, 1362
Henney, C. J., Toussaint, W. A., White, S. M., & Arge, C. N. 2012, *SpWea*, **10**, S02011
Hickmann, K. S., Godinez, H. C., Henney, C. J., & Arge, C. N. 2015, *SoPh*, **290**, 1105
Jiang, J., Cameron, R. H., Schmitt, D., & Schüssler, M. 2011, *A&A*, **528**, A82
Lean, J. L., Wang, Y.-M., & Sheeley, N. R. 2002, *GeoRL*, **29**, 2224
Leighton, R. B. 1969, *ApJ*, **156**, 1
Mackay, D. H., Priest, E. R., & Lockwood, M. 2002a, *SoPh*, **207**, 291
Mackay, D. H., Priest, E. R., & Lockwood, M. 2002b, *SoPh*, **209**, 287
Mackay, D. H., & Yeates, A. R. 2012, *LRSP*, **9**, 6
Mikić, Z., Linker, J. A., Lionello, R., Riley, P., & Titov, V. 2007, in ASP Conf. Ser. 370, Solar and Stellar Physics Through Eclipses, ed. O. Demircan, S. O. Selam, & B. Albayrak (San Francisco, CA: ASP), 299
Muñoz-Jaramillo, A., Senkpeil, R. R., Windmueller, J. C., et al. 2015, *ApJ*, **800**, 48
Nandy, D., Muñoz-Jaramillo, A., & Martens, P. C. H. 2011, *Natur*, **471**, 80
Parker, E. N. 1955, *ApJ*, **122**, 293
Schatten, K. H., Wilcox, J. M., & Ness, N. F. 1969, *SoPh*, **6**, 442
Schou, J., Antia, H. M., Basu, S., et al. 1998, *ApJ*, **505**, 390
Schrijver, C. J. 2001, *ApJ*, **547**, 475
Schrijver, C. J., & De Rosa, M. L. 2003, *SoPh*, **212**, 165
Schrijver, C. J., Kauristie, K., Aylward, A. D., et al. 2015, *AdSpR*, **55**, 2745
Schrijver, C. J., & Zwaan, C. 2000, *CAS*, **34**
Sheeley, N. R., Jr. 1966, *ApJ*, **144**, 723
Snodgrass, H. B. 1983, *ApJ*, **270**, 288
Solanki, S. K. 1993, *SSRv*, **63**, 1
Upton, L., & Hathaway, D. H. 2014, *ApJ*, **780**, 5
van Ballegooijen, A. A., Cartledge, N. P., & Priest, E. R. 1998, *ApJ*, **501**, 866
Wang, Y.-M. 2015, *ApJL*, **803**, L12
Wang, Y.-M., Nash, A. G., & Sheeley, N. R., Jr. 1989, *Sci*, **245**, 712
Wang, Y.-M., & Sheeley, N. R., Jr. 1992, *ApJ*, **392**, 310
Wang, Y.-M., Sheeley, N. R., Jr., & Lean, J. 2000, *GeoRL*, **27**, 621
Wang, Y.-M., Sheeley, N. R., Jr., & Rich, N. B. 2007, *ApJ*, **658**, 1340

⁵ www.cessi.in/solareclipse2017/